

Robust PDE Identification from Noisy Data

Yuchen He ^{*}, Sung Ha Kang [†], Wenjing Liao [‡], Hao Liu [§] and Yingjie Liu [¶]

Abstract

We propose robust methods to identify underlying Partial Differential Equation (PDE) from a given set of noisy time dependent data. We assume that the governing equation is a linear combination of a few linear and nonlinear differential terms in a prescribed dictionary. Noisy data make such identification particularly challenging. Our objective is to develop methods which are robust against a high level of noise, and to approximate the underlying noise-free dynamics well. We first introduce a Successively Denoised Differentiation (SDD) scheme to stabilize the amplified noise in numerical differentiation. SDD effectively denoises the given data and the corresponding derivatives. Secondly, we present two algorithms for PDE identification: Subspace pursuit Time evolution error (ST) and Subspace pursuit Cross-validation (SC). Our general strategy is to first find a candidate set using the Subspace Pursuit (SP) greedy algorithm, then choose the best one via time evolution or cross validation. ST uses multi-shooting numerical time evolution and selects the PDE which yields the least evolution error. SC evaluates the cross-validation error in the least squares fitting and picks the PDE that gives the smallest validation error. We present a unified notion of PDE identification error to compare the objectives of related approaches. We present various numerical experiments to validate our methods. Both methods are efficient and robust to noise.

1 Introduction

In science and engineering, partial differential equations (PDEs) are used to model various real-world scientific phenomena. Numerical solvers for PDEs, as well as analysis on various properties of the solutions have been widely studied in literature. In this paper, we focus on the inverse problem: Given a set of time dependent noisy data, how to identify the governing PDE.

Let the given noisy time dependent discrete data set be \mathbf{D} :

$$\mathbf{D} := \{U_{\mathbf{i}}^n \in \mathbb{R} \mid n = 0, \dots, N; \mathbf{i} = (i_1, \dots, i_d) \text{ with } i_j = 0, \dots, M-1, j = 1, \dots, d\} \text{ for } N, M \in \mathbb{N}, \quad (1)$$

where \mathbf{i} is a d -dimensional spacial index of a discretized domain in \mathbb{R}^d , and n represents the time index at time t^n . The objective is to find an evolutionary PDE of the form

$$\partial_t u = f(u, \partial_{\mathbf{x}} u, \partial_{\mathbf{x}}^2 u, \dots, \partial_{\mathbf{x}}^k u, \dots), \quad (2)$$

^{*}School of Mathematics, Georgia Institute of Technology. Email: royarthur@gatech.edu.

[†]School of Mathematics, Georgia Institute of Technology. Email: kang@math.gatech.edu. Research is supported in part by Simons Foundation grant 282311 and 584960.

[‡]School of Mathematics, Georgia Institute of Technology. Email: wliao60@gatech.edu. Research is supported in part by NSF grant nsf-dms 1818751.

[§]School of Mathematics, Georgia Institute of Technology. Email: hao.liu@math.gatech.edu.

[¶]School of Mathematics, Georgia Institute of Technology. Email: yingjie@math.gatech.edu. Research is supported in part by NSF grants DMS-1522585 and DMS-CDS&E-MSS-1622453.

which represents the dynamics of the given data \mathbf{D} . Here t is the time variable, $\mathbf{x} = [x_1, \dots, x_d] \in \mathbb{R}^d$ denotes the space variable, and $\partial_{\mathbf{x}}^k u = \left\{ \frac{\partial^k u}{\partial x_1^{k_1} \partial x_2^{k_2} \dots \partial x_d^{k_d}} \mid k_1, \dots, k_d \in \mathbb{N}, \sum_{j=1}^d k_j = k \right\}$ is the set of partial derivatives of u with respect to the space variable of order k for $k = 0, 1, \dots$. We assume that f is a polynomial of its arguments, so that the right hand side of (2) is a linear combination of linear and nonlinear differential terms. The model in (2) includes a class of parametric PDEs where the parameters are the polynomial coefficients in f .

Parameter identification in differential equations and dynamical systems has been considered by physicists or applied scientists. Earlier works include [1–4, 26–28], and among which, [2, 26] considered the PDE model as in (2). Two important papers [5, 36] used symbolic regression to recover the underlying physical systems from experimental data. Recently, sparse regression and L_1 -minimization were introduced to promote sparsity in the identification of PDEs or dynamical systems [7, 16, 32, 33]. In [7], Brunton, et al. considered the discovery of nonlinear dynamical systems with sparsity-promoting techniques. The underlying dynamical systems are assumed to be governed by a small number of active terms in a prescribed dictionary, and sparse regression is used to identify these active terms. Several extensions of this sparse regression approach can be found in [15, 20, 25]. In [33], Schaeffer considered the problem of PDE identification using the spectral method, and focused on the benefit of using L_1 -minimization for sparse coefficient recovery. The identification of dynamical systems with highly corrupted and undersampled data are considered in [35, 41]. In [32], Rudy et al. proposed to identify PDEs by solving the L_0 -regularized regression followed by a post-processing step of thresholding. Sparse Bayesian regression was considered in [47] for the recovery of dynamical systems. This series of work focused on the benefit of using L_1 -minimization to resolve dynamical systems or PDEs with certain sparse pattern [34]. Another related problem is to infer the interaction law in a system of agents from the trajectory data. In [6, 23], nonparametric regression was used to predict the interaction function and a theoretical guarantee was established. Another category of methods uses deep learning [17, 21, 22, 24, 29–31].

The most closely related work to this paper is [16], where Identifying Differential Equation with Numerical Time evolution (IDENT) was proposed. It is based on the convergence principle of numerical PDE schemes. LASSO is used to efficiently find a candidate set, and the correct PDE is identified by computing the numerical Time Evolution Error (TEE). Among all the PDEs from the candidate set, the one whose numerical solution best matches the dynamics of the given data is chosen as the identified PDE. When the given data are contaminated by noise, the authors proposed a Least-Square Moving Average method to denoise the data as a pre-processing step. When the coefficients vary in the spatial domain, a Base Element Expansion (BEE) technique was proposed to recover the varying coefficients.

Despite the developments of many effective methods, when the given data is noisy, PDE identification is still challenging. A small amount of noise can make the recovery unstable, especially for high order PDEs. It was shown in [16] that the noise to signal ratio for LASSO depends on the order of the underlying PDE, and IDENT can only handle a small amount of noise when the PDE contains high order derivatives. A major issue is that the numerical differentiation often magnifies noise, which is illustrated by an example in Figure 1.

In this paper, we propose a class of robust methods for PDE identification which can handle a large amount of noise. Our contributions include:

1. First, we propose a new denoising procedure, called Successively Denoised Differentiation (SDD), to stabilize the numerical differentiation applied on noisy data.
2. Second, we present two recovery algorithms which are robust against noise: Subspace pursuit Time evolution (ST) and Subspace pursuit Cross-validation (SC). Both methods utilize the

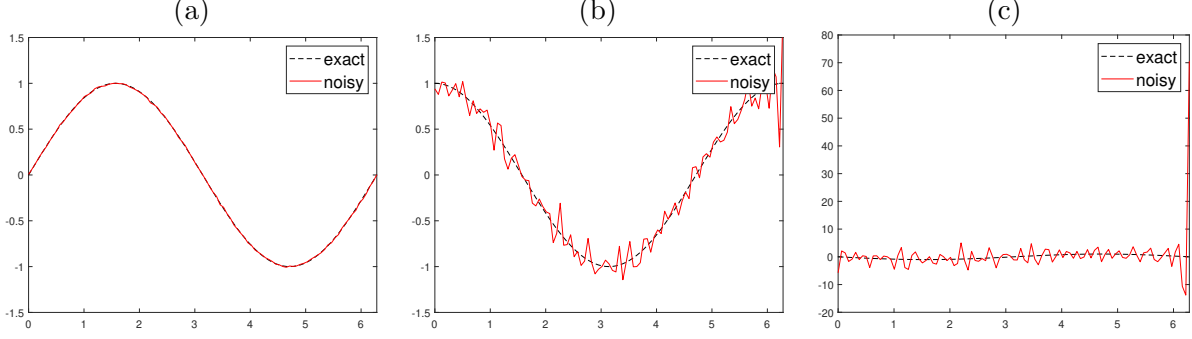


Figure 1: Sensitivity of numerical differentiation to noise. (a) Graph of $\sin(x)$, $0 \leq x \leq 2\pi$ (black), and its noisy version (red) with Gaussian noise of mean 0 and standard deviation 0.007. (b) The first order derivatives of the function (black) and the data (red). (c) The second order derivatives of the function (black) and the data (red). The derivatives of data in (b) and (c) are computed using the five-point ENO scheme. As the order of derivative increases the noise gets amplified.

Subspace Pursuit (SP) greedy algorithm [10] for the selection of a candidate set. ST considers a multi-shooting numerical time evolution error, and SC evaluates the cross-validation error in the least squares fitting. Both methods are efficient and robust against noise. We also present a unified notion of PDE identification error to compare the objectives in related approaches.

This paper is organized as follows. In Section 2, we introduce the PDE identification problem and some notations in Section 2.1 and describe the SDD scheme in Section 2.2. Our proposed ST and SC algorithms are presented in Section 3, and systematic numerical experiments are provided in Section 4. We conclude the paper in Section 5, and some details are discussed in the Appendix.

2 Successively Denoised Differentiation (SDD)

2.1 Data Organization and Notations

Let the time-space domain be $\Omega = [0, T] \times [0, X]^d$ for some $T > 0$ and $X > 0$. Suppose the noisy data \mathbf{D} are given as (1) on a regular grid in Ω , with time index $n = 0, \dots, N$, $N \in \mathbb{N}$ and spatial index $\mathbf{i} \in \mathbb{I}$, where $\mathbb{I} = \{(i_1, \dots, i_d) \mid i_j = 0, \dots, M-1, j = 1, \dots, d, M \in \mathbb{N}\}$. Denote $\Delta t := T/N$ and $\Delta x := X/(M-1)$ as the time and space spacing in the given data, respectively.

At the time t^n and the location $x_{\mathbf{i}}$, each datum is given as

$$U_{\mathbf{i}}^n = u(x_{\mathbf{i}}, t^n) + \varepsilon_{\mathbf{i}}^n, \quad (3)$$

where $t^n := n\Delta t \in [0, T]$, $x_{\mathbf{i}} := (i_1\Delta x, \dots, i_d\Delta x) \in [0, X]^d$, and $\varepsilon_{\mathbf{i}}^n$ is some random noise with mean 0. For $n = 0, 1, \dots, N-1$, we vectorize the data in all spatial domains at time t_n , and denote it as $U^n \in \mathbb{R}^{M^d}$. Concatenating the vectors $\{U^n\}_{n=0}^{N-1}$ vertically gives rise to a long vector $U \in \mathbb{R}^{NM^d}$.

The underlying function f in (2) is assumed to be a finite order polynomial of its arguments:

$$f(u, \partial_{\mathbf{x}}u, \partial_{\mathbf{x}}^2u, \dots, \partial_{\mathbf{x}}^k u, \dots) = c_1 + c_2 \partial_{x_1}u + \dots + c_m u \partial_{x_1}u + \dots \quad (4)$$

where $\partial_{\mathbf{x}}^k$ denotes all k -th order partial derivatives and ∂_{x_i} denotes the partial derivative with respect to the i -th variable. We refer to each term, such as $1, \partial_{x_1}u, \dots, u \partial_{x_1}u, \dots$ in (4), as a *feature*. Since f is a finite order polynomial, only a finite number of features are included. Denote the number

of features by K . Under this model, the function f is expressed in a parametric form as a linear combination of K features. Our objective is to recover the parameters, or coefficients,

$$\mathbf{c} = [c_1 \ c_2 \ \dots \ c_m \ \dots \ c_K]^T \in \mathbb{R}^K.$$

where some of the entries may be zeros.

From \mathbf{D} , we numerically approximate the time and spatial derivatives of u to obtain the following *approximated time derivative vector* $D_t U \in \mathbb{R}^{NM^d}$ and *approximated feature matrix* $F \in \mathbb{R}^{NM^d \times K}$:

$$D_t U = \begin{bmatrix} \frac{U^1 - U^0}{\Delta t} \\ \frac{U^2 - U^1}{\Delta t} \\ \vdots \\ \frac{U^N - U^{N-1}}{\Delta t} \end{bmatrix}, \quad F = \begin{bmatrix} \mathbf{1}_{M^d \times 1} & U^0 & D_{x_1} U^0 & \dots & U^0 \circ D_{x_1} U^0 & \dots \\ \mathbf{1}_{M^d \times 1} & U^1 & D_{x_1} U^1 & \dots & U^1 \circ D_{x_1} U^1 & \dots \\ \vdots & \vdots & \vdots & \ddots & \vdots & \dots \\ \mathbf{1}_{M^d \times 1} & U^{N-1} & D_{x_1} U^{N-1} & \dots & U^{N-1} \circ D_{x_1} U^{N-1} & \dots \end{bmatrix}.$$

In this paper, the time derivatives in $D_t U$ are approximated by the forward difference scheme, and the spatial derivatives in F are computed using the 5-point ENO scheme [13]; $\mathbf{1}_{M^d \times 1}$ denotes the 1-vector of size M^d , and the Hadamard product \circ is the elementwise multiplication between vectors. Each column of F is referred to as a *feature column*. The PDE model in (2) suggests that, an optimal coefficient vector \mathbf{c} should satisfy the following approximation:

$$D_t U \approx F \mathbf{c}. \quad (5)$$

The objective of this paper is to find the correct set of coefficients in (4). Due to a large size of K , the idea of sparsity becomes useful.

Throughout this paper, we denote F_0 as the true feature matrix whose elements are the exact derivatives evaluated at the corresponding time and space location as those in F . For a vector \mathbf{c} , $\|\mathbf{c}\|_p := (\sum_j |c_j|^p)^{\frac{1}{p}}$ is the L_p norm of \mathbf{c} . In particular, $\|\mathbf{c}\|_\infty := \max_j |c_j|$. When $p = 0$, $\|\mathbf{c}\|_0 := \#\{c_j : c_j \neq 0\}$ represents the L_0 semi-norm of \mathbf{c} . The support of \mathbf{c} is denoted by $\text{supp}(\mathbf{c}) := \{j : c_j \neq 0\}$. The vector \mathbf{c} is said to be k -sparse if $\|\mathbf{c}\|_0 = k$ for a non-negative integer k . For any matrix $A_{m \times n}$ and index sets $\mathcal{L}_1 \subseteq \{1, 2, \dots, n\}$, $\mathcal{L}_2 \subseteq \{1, 2, \dots, m\}$, we denote $[A]_{\mathcal{L}_1}$ as the submatrix of A consisting of the columns indexed by \mathcal{L}_1 , and $[A]^{\mathcal{L}_2}$ as the submatrix of A consisting of the rows indexed by \mathcal{L}_2 . A^T , A^* and A^\dagger denote the transpose, conjugate transpose and Moore-Penrose pseudoinverse of A , respectively. For $x \in \mathbb{R}$, $\lfloor x \rfloor$ denotes the largest integer no larger than x .

2.2 Successively Denoised Differentiation (SDD)

As shown in Figure 1, when the given data are contaminated by noise, numerical differentiation amplifies noise and introduces a large error in the time derivative vector $D_t U$ and the approximated feature matrix F . With random noise, the regularity of the given data is different from the regularity of the PDE solution. Thus, denoising plays an important role in PDE identification.

We introduce a smoothing operator S to process the data. Kernel methods are good options for S , such as Moving Average [37] and Moving Least Square (MLS) [18]. In this paper, the smoothing operator S is chosen as the MLS where data are locally fit by quadratic polynomials. In MLS, a weighted least squares problem, along time domain or spacial domain, is solved at each time t^n and

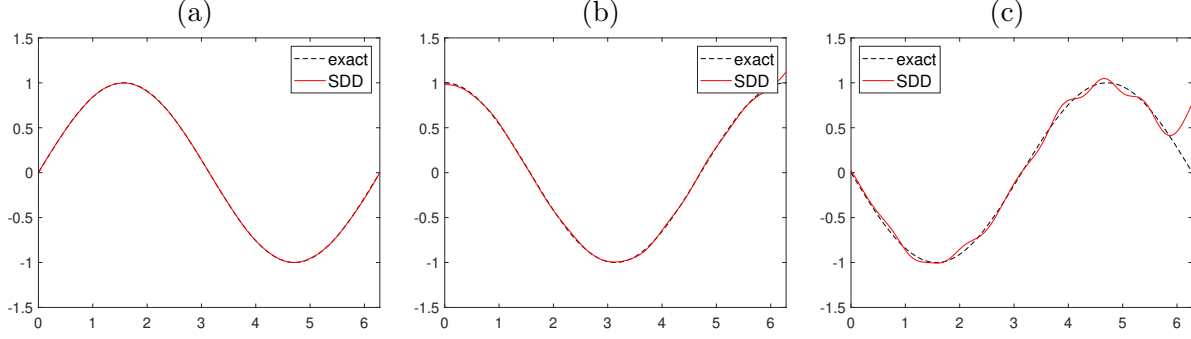


Figure 2: Performance of SDD on the data in Figure 1. (a) Graph of $\sin(x)$, $0 \leq x \leq 2\pi$ (black) and the denoised data (red) using MLS. (b) First order derivatives of the function (black) and the denoised data using SDD (red). (c) Second order derivatives of the function (black) and the denoised data using SDD (red). Derivatives are computed by the five-point ENO scheme, and the smoothing operator S is MLS.

spatial location x_i as follows:

$$S_{(\mathbf{x})}[U_i^n] = p_i^n(x_i), \text{ where } p_i^n = \arg \min_{p \in P_2} \sum_{\mathbf{j} \in \mathbb{I}} (p(x_j) - U_j^n)^2 \exp\left(-\frac{\|x_i - x_j\|^2}{h^2}\right),$$

$$S_{(t)}[U_i^n] = p_i^n(t^n), \text{ where } p_i^n = \arg \min_{p \in P_2} \sum_{0 \leq k \leq N} (p(t^k) - U_i^k)^2 \exp\left(-\frac{\|t^n - t^k\|^2}{h^2}\right).$$

Here $h > 0$ is a width parameter of the kernel, and P_2 denotes the set of polynomials of degree no more than 2. When $d = 1$, it was shown that if $\{U_j^n\}_{j=1}^M$ is a third order approximation of a smooth function $u(x, t^n)$ with or without noise, and if h is appropriately chosen, MLS gives a third order approximation of $u(x, t^n)$ [16, 44]. This result can be easily generalized to higher order polynomials.

We propose a Successively Denoised Differentiation (SDD) procedure to stabilize the numerical differentiation. For every derivative approximation, smoothing is applied as follows:

Successively Denoised Differentiation (SDD)	
$u \approx S_{(\mathbf{x})}[U]$	The given data set U is denoised by MLS.
$\partial_t u \approx S_{(t)} D_t S_{(\mathbf{x})}[U]$	Denoising at numerical time differentiation.
$\partial_{\mathbf{x}}^k u \approx (S_{(\mathbf{x})} D_{x_1})^{k_1} \cdots (S_{(\mathbf{x})} D_{x_d})^{k_d} S_{(\mathbf{x})}[U]$, where $\sum_{i=1}^d k_i = k$, for $k = 1, 2, \dots$	Denoising at every spatial numerical differentiation step.

All nonlinear features and mixed-partial derivatives are computed by the operations above. The main idea of SDD is to smooth the data at each step (before and) after the numerical differentiation. This simple idea effectively stabilizes numerical differentiation. Figure 2 shows the results of SDD for the same data in Figure 1. The approximations of the first and second order derivatives of u are greatly improved.

In Section 4.6, we explore details of SDD when different smoothing operators are used. We find that MLS has the best performance in terms of preserving the derivative profiles. We set S to be MLS for the numerical experiments.

To simplify the notations, in the rest of this paper, we use U to denote the denoised data $S_{(\mathbf{x})}[U]$, and $D_t U$ as well as $D_{\mathbf{x}}^k U$ to denote the numerical derivatives with SDD applied as above.

3 Proposed Methods: ST and SC

Under the parametric model in (4), the PDE identification problem can be reduced to solving the linear system (5) for a sparse vector \mathbf{c} with few nonzero entries. Sparse regression can be formulated as the following L_0 -minimization

$$\min \|\mathbf{c}\|_0, \quad \text{subject to } \|F\mathbf{c} - D_t U\| \leq \epsilon, \quad (6)$$

for some $\epsilon > 0$. However, the L_0 -minimization in (6) is NP hard. Its approximate solutions have been intensively studied in literature. The most popular surrogate for the L_0 semi-norm is the L_1 norm as applied in image and signal processing [8, 11]. The L_1 -regularized minimization is called Least Absolute Shrinkage and Selection Operator (LASSO) [39], which was used in [16, 32, 33] for PDE identification. The common strategy in these works is to utilize LASSO to select a candidate set, then refine the results with other techniques.

In this paper, we utilize a greedy algorithm called Subspace Pursuit (SP) [10] to select a candidate set. Different from LASSO, SP takes the sparsity level as the input. Let k be a positive integer and denote $\mathbf{b} = D_t U$. For a fixed sparsity level k , $\text{SP}(k; F, \mathbf{b})$ in Algorithm 1 gives rise to a k -sparse vector whose support is selected in a greedy fashion. It was proved that SP gives rise to a solution of the L_0 -minimization (6) under certain conditions of the matrix F , such as the restricted isometry property [10].

Algorithm 1: Subspace Pursuit $\text{SP}(k; F, \mathbf{b})$

Input: $F \in \mathbb{R}^{NM^d \times K}$, $\mathbf{b} \in \mathbb{R}^{NM^d}$ and sparsity $k \in \mathbb{N}$.

Initialization: $j = 0$;

$G \leftarrow$ column-normalized version of F ;

$\mathcal{I}^0 = \{k \text{ indices corresponding to the largest magnitude entries in the vector } G^* \mathbf{b}\}$;

$\mathbf{b}_{\text{res}}^0 = \mathbf{b} - G_{\mathcal{I}^0} G_{\mathcal{I}^0}^\dagger \mathbf{b}$.

while *True* **do**

Step 1. $\tilde{\mathcal{I}}^{j+1} = \mathcal{I}^j \cup \{k \text{ indices corresponding to the largest magnitude entries in the vector } G^* \mathbf{b}_{\text{res}}^j\}$;

Step 2. Set $\mathbf{c}_p = G_{\tilde{\mathcal{I}}^{j+1}}^\dagger \mathbf{b}$;

Step 3. $\mathcal{I}^{j+1} = \{k \text{ indices corresponding to the largest elements of } \mathbf{c}_p\}$;

Step 4. Compute $\mathbf{b}_{\text{res}}^{j+1} = \mathbf{b} - G_{\mathcal{I}^{j+1}} G_{\mathcal{I}^{j+1}}^\dagger \mathbf{b}$;

Step 5. If $\|\mathbf{b}_{\text{res}}^{j+1}\|_2 > \|\mathbf{b}_{\text{res}}^j\|_2$, let $\mathcal{I}^{j+1} = \mathcal{I}^j$ and terminate the algorithm; otherwise set $j \leftarrow j + 1$ and iterate.

Output: $\hat{\mathbf{c}} \in \mathbb{R}^K$ satisfying $\hat{\mathbf{c}}_{\mathcal{I}_j} = F_{\mathcal{I}_j}^\dagger \mathbf{b}$ and $\hat{\mathbf{c}}_{(\mathcal{I}_j)^c} = \mathbf{0}$.

We propose two new methods based on SP for PDE identification: Subspace pursuit Time evolution (ST) and Subspace pursuit Cross-validation (SC). ST uses multi-shooting numerical time evolution and selects the PDE which yields the least evolution error. From a different perspective, SC computes the cross-validation error in the least squares fitting and picks the PDE that gives the smallest error.

3.1 Subspace Pursuit Time Evolution (ST)

We first propose a method combining SP and the idea of time evolution. In [16], Time Evolution Error (TEE) quantifies the mismatch between the solution simulated from a candidate PDE and the denoised data. Any candidate coefficient vector $\hat{\mathbf{c}} = (\hat{c}_1, \hat{c}_2, \dots)$ defines a candidate PDE: $u_t = \hat{c}_1 + \hat{c}_2 \partial_{x_1} u + \dots + \hat{c}_m u \partial_{x_1} u + \dots$. This PDE is numerically evolved from the initial condition U^0 with a smaller time step $\hat{\Delta}t \ll \Delta t$. Denote $\hat{U}^1, \hat{U}^2, \dots, \hat{U}^N$ as this numerical solution at the same time-space location as U^1, U^2, \dots, U^N . The TEE of the candidate PDE given by $\hat{\mathbf{c}}$ is

$$\text{TEE}(\hat{\mathbf{c}}) = \frac{1}{N} \sum_{n=1}^N \|\hat{U}^n - U^n\|_2,$$

where U^n is the denoised data at time t^n . When there are several candidate PDEs, the one with the least TEE is picked [16]. This TEE idea is based on the convergence principle that a correct numerical approximation converges to the true solution as the time step $\hat{\Delta}t$ goes to zero. The error from the wrongly identified terms grows during this time evolution process. Figure 3 (a) and (b) illustrate the idea of TEE.

In this paper, we propose a *Multi-shooting Time Evolution Error* (MTEE). The idea is to evolve a candidate PDE from multiple time locations with a time step $\hat{\Delta}t \ll \Delta t$ using the forward Euler scheme for a time length of $w\Delta t$, where w is a positive integer. Throughout this paper, we use $\hat{\Delta}t = \Delta t/5$. Let $\hat{U}^{(n+w)|n}$ be the numerical solution of the candidate PDE at the time $(n+w)\Delta t$, which is evolved from the initial condition U^n at time $t^n = n\Delta t$. The MTEE is defined as

$$\text{MTEE}(\hat{\mathbf{c}}; w) = \frac{1}{N-w} \sum_{n=0}^{N-1-w} \|\hat{U}^{(n+w)|n} - U^{n+w}\|_2. \quad (7)$$

Figure 3 (c) and (d) demonstrate the process of multi-shooting time evolution. While the TEE evolution starts from the initial condition U^0 and ends at T , the MTEE evolution starts from various time locations, such as $t^n, n = 0, \dots, N-1-w$, and lasts for a shorter time, e.g. $w\Delta t$ in our case.

MTEE has two advantages over TEE: (1) MTEE is more robust against noise in comparison with TEE. If $w \ll N$, the noise accumulates for less time, which helps to stabilize numerical solvers; (2) MTEE is more flexible and its computation is parallelizable.

The SP algorithm finds a coefficient vector with a specified sparsity, but it is difficult to know the correct sparsity from the given data. We propose *Subspace pursuit Time evolution* (ST) which iteratively refines the selection of features.

As an initial condition, we set $K_0 = K$ and $\mathcal{A}_0 = \{1, \dots, K\}$. At the first iteration, all possible sparsity levels are considered in the SP algorithm. For each $k = 1, \dots, K$, we run $\text{SP}(k; F, D_t U)$ to obtain a coefficient vector $\hat{\mathbf{c}}^{(k)} \in \mathbb{R}^K$ such that $\|\hat{\mathbf{c}}^{(k)}\|_0 = k$, which gives rise to the PDE:

$$u_t = f_{\text{SP}(k)} \text{ where } f_{\text{SP}(k)} := \hat{c}_1^{(k)} + \hat{c}_2^{(k)} \partial_{x_1} u + \dots + \hat{c}_m^{(k)} u \partial_{x_1} u + \dots. \quad (8)$$

We then numerically evolve each PDE $u_t = f_{\text{SP}(k)}$, for $k = 1, \dots, K$ and calculate the corresponding MTEE. Among these PDEs, the one with the smallest MTEE is selected, then let

$$K_1 = \arg \min_{k=1,2,\dots,K} \text{MTEE}(\hat{\mathbf{c}}^{(k)}; w) \text{ and } \mathcal{A}_1 = \text{supp}(\hat{\mathbf{c}}^{(K_1)}).$$

If $\mathcal{A}_1 = \mathcal{A}_0$, the algorithm is terminated; otherwise, we continue to the second iteration.

At the second iteration, we refine the selection from the index set \mathcal{A}_1 with cardinality K_1 . For $k = 0, \dots, K_1$, we run $\text{SP}(k; [F]_{\mathcal{A}_1}, D_t U)$ to obtain a coefficient vector $\hat{\mathbf{c}}^{(k)} \in \mathbb{R}^K$ such that

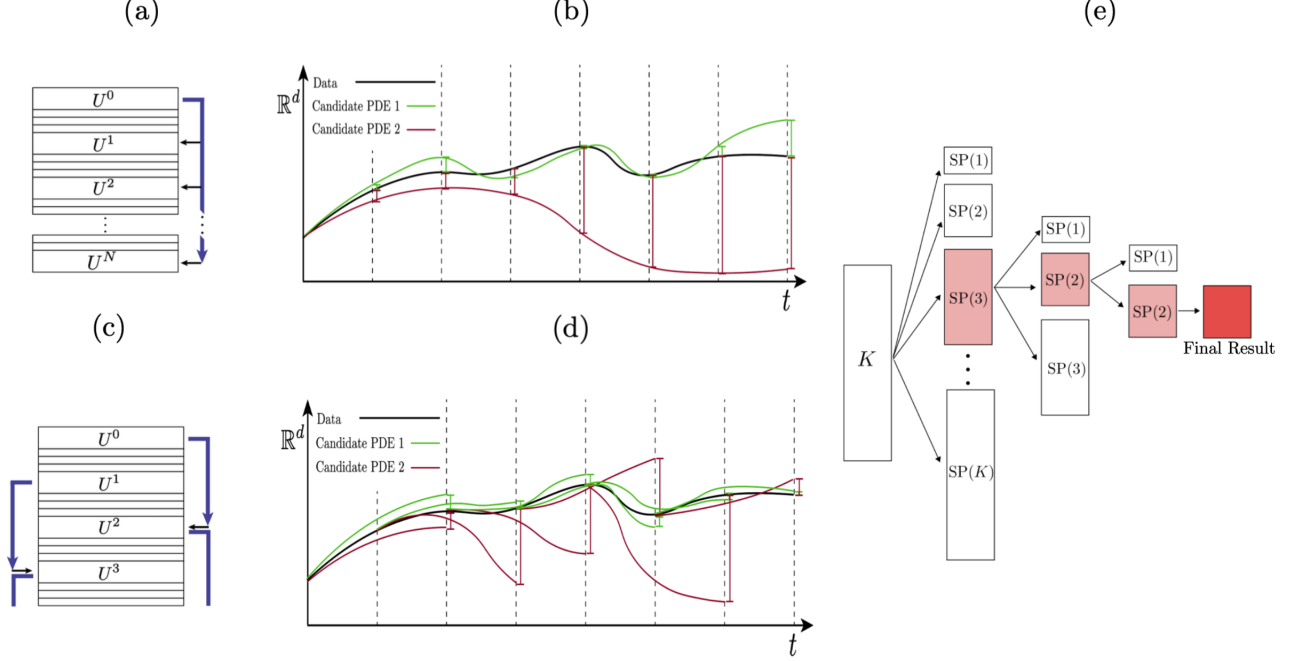


Figure 3: (a) and (b) illustrate the idea of TEE. (c) and (d) explain MTEE when $w = 2$. The blue arrows in (a) and (c) represent time evolution using the forward Euler scheme on a fine time grid with spacing $\widetilde{\Delta t} \ll \Delta t$. In (b), two different PDEs (green and red) are evolved, and the green one has a smaller TEE. In (d) the candidate PDEs are evolved from multiple time locations, and their numerical solutions are compared with the denoised data after a time length of $w\Delta t$. (e) An example of the ST iteration. Starting with a large number K , the first iteration gives rise to K candidate coefficients for $k = 1, \dots, K$. The PDE with the smallest MTEE is picked, e.g. $SP(3)$ with cardinality $K_1 = 3$ and support \mathcal{A}_1 . The second iteration gives rise to the candidate coefficients only supported on \mathcal{A}_1 using $SP(k)$ with $k = 1, 2, 3$. The PDE with the smallest MTEE is found, e.g. $SP(2)$ with cardinality $K_2 = 2$ and support \mathcal{A}_2 . The third iteration does not change the support, i.e. $\mathcal{A}_3 = \mathcal{A}_2$, so the final output is the coefficient vector of $SP(2)$.

$$\widehat{\mathbf{c}}_{\mathcal{A}_1}^{(k)} = SP(k; [F]_{\mathcal{A}_1}, D_t U), \text{ and } \widehat{\mathbf{c}}_{\mathcal{A}_1^c}^{(k)} = \mathbf{0},$$

and the associated PDE $u_t = f_{SP(k)}$ as in (8). Among these PDEs, the one with the smallest MTEE is selected, and we denote

$$K_2 = \arg \min_{k=1,2,\dots,K_1} \text{MTEE}(\widehat{\mathbf{c}}^{(k)}; w), \text{ and } \mathcal{A}_2 = \text{supp}(\widehat{\mathbf{c}}^{(K_1)}).$$

If $\mathcal{A}_2 = \mathcal{A}_1$, the algorithm is terminated; otherwise, we continue to the next iteration in a similar manner.

The ST iteration will be terminated when the index set remains the same, i.e., $\mathcal{A}_j = \mathcal{A}_{j+1}$. The ST outputs a recovered coefficient vector and the corresponding PDE denoted by $ST(w)$. A complete description of ST is given in Algorithm 2, and Figure 3 (e) illustrates an example of the ST iteration.

Algorithm 2: Subspace pursuit Time evolution (ST)

Input: $F \in \mathbb{R}^{NM^d \times K}$, $D_t U \in \mathbb{R}^{NM^d}$ and a positive integer w .

Initialization: $j = 0$, $K_0 = K$ and $\mathcal{A}_0 = \{1, 2, \dots, K\}$.

while $\mathcal{A}_{j+1} \neq \mathcal{A}_j$ **do**

Step 1. For $k = 1, 2, \dots, K_j$, run SP($k; [F]_{\mathcal{A}_j}, D_t U$) to obtain a coefficient vector

$\hat{\mathbf{c}}^{(k)} \in \mathbb{R}^K$ such that

$$\hat{\mathbf{c}}_{\mathcal{A}_j}^{(k)} = \text{SP}(k; [F]_{\mathcal{A}_j}, D_t U) \text{ and } \hat{\mathbf{c}}_{\mathcal{A}_j^c}^{(k)} = \mathbf{0},$$

 and the associated PDE $u_t = f_{\text{SP}(k)}$ given in (8).

Step 2. Among all the PDEs $u_t = f_{\text{SP}(k)}$ for $k = 1, \dots, K_j$, select the one with the minimum MTEE($\hat{\mathbf{c}}^{(k)}; w$) and update

$$K_{j+1} = \arg \min_{k=1,2,\dots,K_j} \text{MTEE}(\hat{\mathbf{c}}^{(k)}; w) \text{ and } \mathcal{A}_{j+1} = \text{supp}(\hat{\mathbf{c}}^{(k_{j+1})}).$$

 If $\mathcal{A}_{j+1} = \mathcal{A}_j$, terminate the algorithm; otherwise, update $j = j + 1$.

Output: Recovered coefficient $\hat{\mathbf{c}}^{K_{j+1}}$ and the corresponding PDE, denoted by ST(w).

3.2 Subspace Pursuit Cross Validation (SC)

Our second method utilizes the idea of cross validation for the linear system in (5). Cross-validation is commonly used in statistics for the choice of parameters in order to avoid overfitting [14]. We consider the two-fold cross validation where data are partitioned into two subsets. One subset is used to estimate the coefficient vector and the other one is used to validate the candidates. If a good coefficient vector is found within one subset, it should yield a small validation error for the other subset because of consistency.

For some fixed ratio parameter $\alpha \in (0, 1)$, we split the rows of $D_t U \in \mathbb{R}^{NM^d}$ (and $F \in \mathbb{R}^{NM^d \times K}$) into two groups indexed by \mathcal{T}_1 and \mathcal{T}_2 , such that \mathcal{T}_1 consists of the indices of the first $\lfloor \alpha NM^d \rfloor$ rows and \mathcal{T}_2 consists of the indices of the rest of the rows. Since we focus on PDEs with constant coefficients, the idea of cross validation is applicable: if a correct support is identified, the coefficient vector obtained from the data in \mathcal{T}_1 should be compatible with the data in \mathcal{T}_2 .

We introduce our *Subspace pursuit Cross validation (SC)* algorithm where cross validation is incorporated into the SP algorithm. SC consists of the following three steps:

Step 1: For each sparsity level $k = 1, 2, \dots, K$, use SP to select a set of active features:

$$\mathcal{A}_k = \text{supp}(\text{SP}(k; F, D_t U)).$$

Step 2: Use the data in \mathcal{T}_1 to compute the estimator for the coefficient vector, $\hat{\mathbf{c}}^{(k)} \in \mathbb{R}^K$, by the following least squares problem

$$\hat{\mathbf{c}}^{(k)} = \arg \min_{\mathbf{c} \in \mathbb{R}^K \text{ such that } \mathbf{c}_{\mathcal{A}_k^c} = 0} \|[F]_{\mathcal{A}_k}^{\mathcal{T}_1} \mathbf{c}_{\mathcal{A}_k} - [D_t U]^{\mathcal{T}_1}\|_2^2,$$

and then use the data in \mathcal{T}_2 to compute a Cross validation Estimation Error (CEE)

$$\text{CEE}(\mathcal{A}_k; \alpha, \mathcal{T}_1, \mathcal{T}_2) = \|[D_t U]^{\mathcal{T}_2} - [F]^{\mathcal{T}_2} \hat{\mathbf{c}}^{(k)}\|_2. \quad (9)$$

Step 3: Set $k_{\min} = \arg \min_k \text{CEE}(\mathcal{A}_k; \alpha, \mathcal{T}_1, \mathcal{T}_2)$ and the estimated coefficient vector is given as

$$\hat{\mathbf{c}} = \arg \min_{\mathbf{c} \in \mathbb{R}^K \text{ such that } \mathbf{c}_{\mathcal{A}_k^c} = 0} \|[F]_{\mathcal{A}_{k_{\min}}}^{\mathcal{T}_1} \mathbf{c}_{\mathcal{A}_{k_{\min}}} - [D_t U]^{\mathcal{T}_1}\|_2^2.$$

Algorithm 3: Subspace pursuit Cross validation (SC) Algorithm

Input: $F \in \mathbb{R}^{NM^d \times K}$ and $D_t U \in \mathbb{R}^{NM^d}$; $0 < \alpha < 1$ ratio of the training data.

Step 1. For $k = 1, 2, \dots, K$, run $\text{SP}(k; F, D_t U)$ to obtain the support of the candidate coefficients

$$\mathcal{A}_k = \text{supp}(\text{SP}(k; F, D_t U)) .$$

Step 2. For each k , compute the averaged cross validation error

$$\text{CEE}(\mathcal{A}_k, \alpha) = \frac{1}{2} (\text{CEE}(\mathcal{A}_k; \alpha, \mathcal{T}_1, \mathcal{T}_2) + \text{CEE}(\mathcal{A}_k; 1 - \alpha, \mathcal{T}_2, \mathcal{T}_1)) .$$

Step 3. Choose the k which gives the smallest cross validation error and denote it by k_{\min}

$$k_{\min} = \arg \min_k \text{CEE}(\mathcal{A}_k, \alpha) .$$

Estimate the coefficients by least squares as

$$\hat{\mathbf{c}} = \arg \min_{\mathbf{c} \in \mathbb{R}^K \text{ such that } \mathbf{c}_{\mathcal{A}_k^c} = 0} \left\| [F]_{\mathcal{A}_{k_{\min}}}^{\mathcal{T}_1} \mathbf{c}_{\mathcal{A}_{k_{\min}}} - [D_t U]^{\mathcal{T}_1} \right\|_2^2 .$$

Output: Recovered coefficient $\hat{\mathbf{c}}$ and the identified PDE denoted by $\text{SC}(\alpha)$.

The identified PDE by SC is denoted as $\text{SC}(\alpha)$.

CEE in (9) is an effective measure for consistency. If the support of the estimated coefficient vector matches that of the true one, CEE is guaranteed to be small provided with sufficiently high resolution in time and space.

Theorem 3.1. Assume that $D_t U \rightarrow u_t$ and $F \rightarrow F_0$ as $\Delta t, \Delta x \rightarrow 0$. Let $\mathcal{A}_0 = \text{supp}(\mathbf{c}_0)$ where \mathbf{c}_0 is the coefficient vector of the true PDE. For any set of support \mathcal{A} , we have

$$\text{CEE}(\mathcal{A}; \alpha, \mathcal{T}_1, \mathcal{T}_2) \leq \left\| \left([F_0]_{\mathcal{A}_0}^{\mathcal{T}_2} ([F_0]_{\mathcal{A}_0}^{\mathcal{T}_1})^\dagger - [F_0]_{\mathcal{A}}^{\mathcal{T}_2} ([F_0]_{\mathcal{A}}^{\mathcal{T}_1})^\dagger \right) [u_t]^{\mathcal{T}_1} \right\|_2 + g(\mathcal{A}; \alpha, \mathcal{T}_1, \mathcal{T}_2) ,$$

where $g > 0$ is a positive function independent of \mathcal{A}_0 , such that $g \rightarrow 0$ as $\Delta t, \Delta x \rightarrow 0$.

Proof. See Appendix B. □

In (9), the data in \mathcal{T}_1 serve as the training set, and the data in \mathcal{T}_2 act as the validation set. One can also use the data in \mathcal{T}_2 for training and the data in \mathcal{T}_1 for validation, which gives rise to the cross validation estimation error $\text{CEE}(\mathcal{A}_k; 1 - \alpha, \mathcal{T}_2, \mathcal{T}_1)$. To improve the robustness of SC, we replace (9) with the following averaged cross validation error:

$$\text{CEE}(\mathcal{A}_k, \alpha) = \frac{1}{2} (\text{CEE}(\mathcal{A}_k; \alpha, \mathcal{T}_1, \mathcal{T}_2) + \text{CEE}(\mathcal{A}_k; 1 - \alpha, \mathcal{T}_2, \mathcal{T}_1)) .$$

In general, one can randomly pick part of the data as the training set and use the rest as the validation set. For simplicity, we split the data according to the row index in this paper.

The proposed SC algorithm is summarized in Algorithm 3. In comparison with ST, SC does not involve any numerical evolution of the candidate PDE, so the computation of SC is faster.

3.3 Comparison with Related Methods

In this section, we discuss the error representation to compare different objective of PDE identification approaches. We consider two ways to measure errors in PDE identification. The first one is the error between the identified numerical solution \hat{U} and the exact solution u , which is given by $e(u) := \hat{U} - u$. The second error is $e(u_t) := D_t\hat{U} - u_t$, which measures the difference between the numerical time derivative of \hat{U} and the ground truth u_t . The errors $e(u)$ and $e(u_t)$ are closely related, which is explained in details in Appendix A.

Many existing methods for the identification of PDEs or dynamical systems involve a minimization of $e(u)$ or $e(u_t)$. Consider the following decomposition of $e(u)$:

$$e(u) = \underbrace{\hat{U} - U}_{\text{Data fidelity}} + \underbrace{U - u}_{\text{Measurement error}}, \quad (10)$$

where U is the given data. In (10), the *Data fidelity* $\hat{U} - U$ represents the accuracy of the identified PDE in comparison with the given data U . In literature, a class of dynamic-fitting approaches such as [1, 4, 26, 36] focus on controlling the data fidelity error in order to ensure if the numerical prediction is consistent with the evolution of the given data. The *Measurement error* $U - u$ comes from data acquisition where the given data are contaminated by noise. Denoising is an important step to reduce the measurement error.

The second error $e(u_t)$ can be expressed as

$$e(u_t) = \underbrace{D_t\hat{U} - D_tU}_{\text{Response error}} + \underbrace{D_tU - F\hat{\mathbf{c}}}_{\text{Regression error}} + \underbrace{F(\hat{\mathbf{c}} - \mathbf{c}_0)}_{\text{Coefficient error}} + \underbrace{(F - F_0)\mathbf{c}_0}_{\text{System error}}. \quad (11)$$

where $\hat{\mathbf{c}}$ is the estimated coefficient. The first term $D_t\hat{U} - D_tU$ is called the *Response error*, which is the difference between the numerical derivatives of the identified PDE and the given data. The L_2 norm of the *Regression error* $D_tU - F\hat{\mathbf{c}}$ is the most frequently used objective function in PDE identification for the regression-based methods [2, 3, 19, 28, 42]. In addition, one can introduce various types of regularization, such as the L_1 regularization [16, 32, 33] to induce sparsity. The *coefficient error* $F(\hat{\mathbf{c}} - \mathbf{c}_0)$ compares $\hat{\mathbf{c}}$ and \mathbf{c}_0 . This term vanishes when $\hat{\mathbf{c}} - \mathbf{c}_0$ lies in the null space of F , which can occur even when $\hat{\mathbf{c}} \neq \mathbf{c}_0$. If the initial condition of the PDE is too simple, the null space of F is very large, which makes the PDE identification problem ill-posed. See Equation (16) and (17) for an example. In order to guarantee a successful identification, the initial condition should have sufficient variations so that F satisfies an incoherence or null space property [12]. The final term $(F - F_0)\mathbf{c}_0$ represents the *System error*, which is due to the numerical differentiation in the computation of F . Our SDD denoising technique can effectively reduce the system error.

We summarize in Table 1 the objectives considered by many existing methods in the literature. These methods are categorized according to which error term(s) that they aim at minimizing. As for our proposed methods, ST minimizes the data fidelity, and SC focuses on the coefficient error and the regression error for the PDE identification.

4 Numerical Experiments

In this section, we perform a systematic numerical study to demonstrate the effectiveness of ST and SC and compare them to IDENT [16]. To measure the identification error, we use the following relative coefficient error e_c and grid-dependent residual error e_r :

$$e_c = \frac{\|\hat{\mathbf{c}} - \mathbf{c}\|_1}{\|\mathbf{c}\|_1}, \quad e_r = \begin{cases} \sqrt{\Delta x \Delta t} \|F(\hat{\mathbf{c}} - \mathbf{c})\|_2 & \text{for one dimensional PDE.} \\ \sqrt{\Delta x \Delta y \Delta t} \|F(\hat{\mathbf{c}} - \mathbf{c})\|_2 & \text{for two dimensional PDE.} \end{cases}.$$

Type of Problems	Objectives in Minimization	Methods
Parameter Estimation	Data fidelity	[1, 4, 26, 27, 36, 40]
	Regression error	[2, 3, 19, 28, 42]
	Regression error + Data fidelity	[46]
Model Identification	Data fidelity	[22]
	Regression error	[32, 33]
	Regression error + Data fidelity	ST (Section 3.1), [16]
	Regression error + Coefficient error	SC (Section 3.2)

Table 1: Comparison of the objectives of PDE identification. For parameter estimation problems, the feature variables of the underlying PDEs are known. For model identification problems, such active set is unknown; hence sparsity is often imposed, or neural network is designed.

The relative coefficient error e_c measures the accuracy in the recovery of PDE coefficients, while the residual error e_r measures the difference between the learned dynamics and the denoised one by SDD. Since each feature vector in F may have different scales, e_r can be different from e_c in some cases. Especially when the given data contain noise, the features containing higher order derivatives have greater magnitudes compared to the features containing lower order derivatives. In this case, a small coefficient error in the high order terms may lead to a large e_r . We use both e_c and e_r to quantify the PDE identification error.

To generate the data, we first solve the underlying PDE by forward Euler scheme using time and space step δt and δx respectively, then downsample the data to then we add Gaussian noise with standard deviation σ to the clean data. We say that the noise is $p\%$ when setting $\sigma = \frac{p}{100} \sqrt{\frac{1}{NM^d} \sum_n \sum_i (u(\mathbf{x}_i, t^n))^2}$. In the computation of $D_t U$ and the feature matrix F , we always use SDD with MLS with $h = 0.04$ as the smoother. When MLS is used to denoise the data of two dimensional PDEs, one can either fit two dimensional polynomials or fit one dimensional polynomials in each dimension. In this work, we use the second approach. In ST, $\tilde{\Delta t} = \Delta t/5$ is used.

In our experiments, we consider PDEs containing partial derivatives up to the second order and f being a polynomial with degree up to 2. We consider 10 features $1, u, u^2, u_x, u_x^2, uu_x, u_{xx}, u_{xx}^2, uu_{xx}$, and $u_x u_{xx}$ as the dictionary for one dimensional PDEs and 28 for two dimensional PDEs, which exhaust all the available features up to order 2 and degree 2, e.g., $u_{xx} u_y$ and $u_{xy} u_{yy}$.

4.1 Transport Equation

Our first experiment is a transport equation with zero Dirichlet boundary condition:

$$u_t = -u_x, \quad (12)$$

with an initial condition of

$$u(0, x) = \begin{cases} \sin^2(2\pi x/(1-T)) \cos(2\pi x/(1-T)), & \text{for } 0 \leq x \leq 1-T, \\ 0, & \text{otherwise} \end{cases},$$

for $0 < t \leq T$. The given data \mathbf{D} is generated by explicitly solving (12) with $\delta x = \Delta x = 1/256$, $\delta t = \Delta t = 10^{-3}$ and $T = 0.05$.

Table 2 shows the results of ST(20) and SC(1/200) with various noise levels. In practice we have no a priori knowledge of whether the given data contain noise, so we conduct two experiments with and without SDD to check the effect of SDD on clean data. We observe that SDD makes a

Method	Identified PDE, 0% noise without SDD	e_c	e_r
ST(20)	$u_t = -0.9994u_x$	6.20×10^{-4}	4.89×10^{-4}
SC(1/200)	$u_t = -0.9993u_x - 0.0010u_{xx}$	1.65×10^{-3}	1.11×10^{-2}
	0% noise with SDD	e_c	e_r
ST(20)	$u_t = -0.9997u_x$	3.36×10^{-4}	2.64×10^{-4}
SC(1/200)	$u_t = -0.9997u_x - 0.0010u_{xx}$	1.34×10^{-3}	1.11×10^{-2}
	10% noise	e_c	e_r
ST(20) and SC(1/200)	$u_t = -1.0357u_x$	3.57×10^{-2}	2.67×10^{-2}
	30% noise	e_c	e_r
ST(20) and SC(1/200)	$u_t = -0.9421u_x$	5.79×10^{-2}	4.31×10^{-2}

Table 2: Identification of the transport equation (12) with different noise levels. In the noise-free case, applying SDD does not introduce strong bias. The identification results by ST and SC are stable even with 30% noise.

small difference in the noise-free case. With clean data, SC identifies an additional u_{xx} term with a small coefficient, while ST is capable of ruling out all wrong terms. The corresponding e_c and e_r are both small. With 10% or 30% noise, both ST and SC identify the same PDE with small e_c and e_r values.

To demonstrate the significance of SDD and the effectiveness of ST and SC, we display the noisy data with 10% and 30% noise, the denoised data, and the recovered dynamics in Figure 4. Even though the given data contain a large amount of noise, the recovered dynamics are close to the clean data.

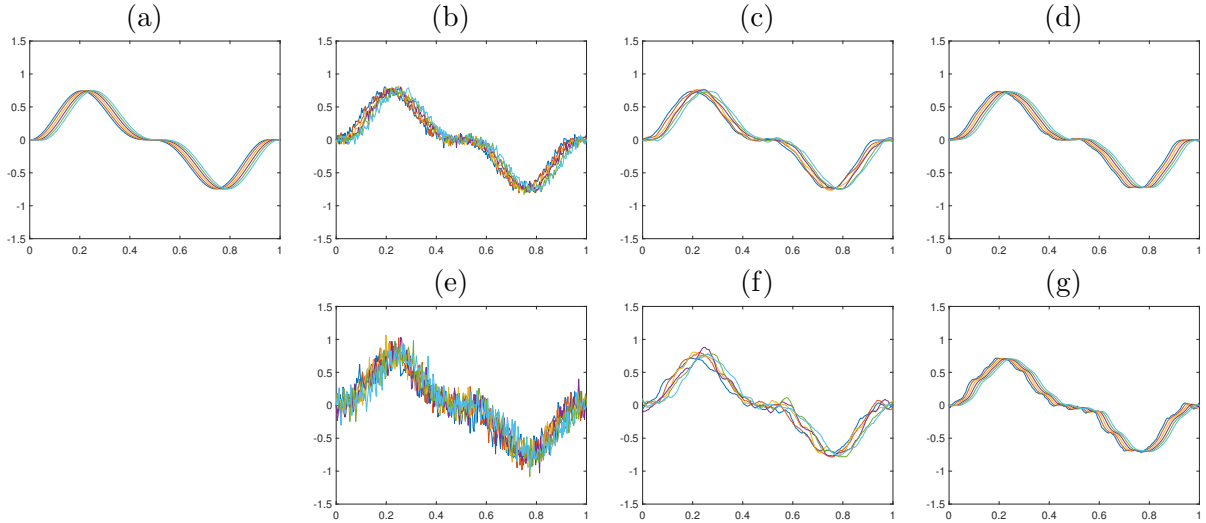


Figure 4: Noisy and denoised data of the transport equation (12), as well as simulations of the recovered PDE. (a) The clean data, (b) data with 10% noise, (c) the denoised data $S_{\mathbf{x}}[U]$, (d) simulation of the PDE identified by ST and SC (identical). (e) Data with 30% noise, (f) the denoised data $S_{(\mathbf{x})}[U]$, and (g) simulation of the PDE identified by ST and SC (identical).

Figure 5 shows how e_c and e_r change when the noise level varies from 0.1% to 100%. Each experiment is repeated 50 times and the error is averaged. We test IDENT, ST(20) and SC(1/200). Figure 5 (a) shows that the e_c of ST or SC is much smaller than that of IDENT as the noise level is larger than 20%. Figure 5 (b) shows e_r versus noise. The coefficient error e_c by ST and SC is

significantly smaller than that of IDENT.

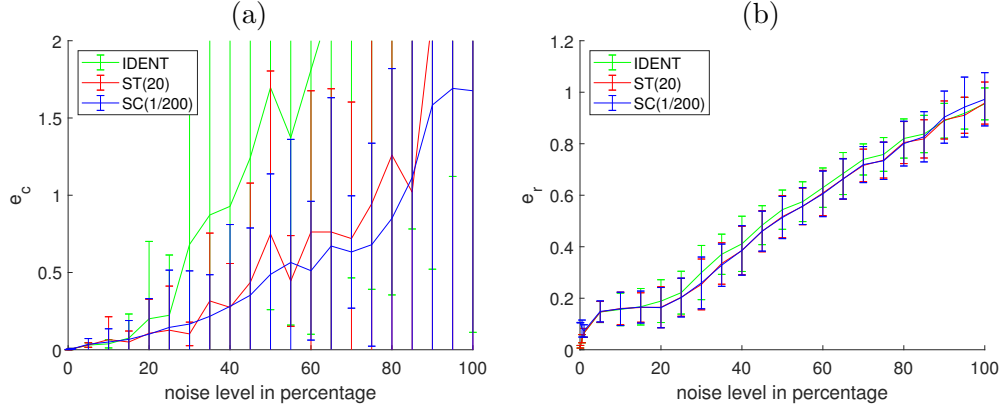


Figure 5: The average error e_c and e_r over 50 experiments of the transport equation (12) with respect to various noise levels. (a) The curve represents the average e_c for IDENT [16] (Green), ST (Red) and SC (Blue), and the standard deviation is represented by vertical bars. (b) The average and variation of e_r for IDENT (Green), ST (Red) and SC (Blue). The coefficient error e_c by ST and SC is significantly smaller than that of IDENT.

In Figure 6, we explore the robustness of SC with respect to the choice of α . We present e_c and e_r versus $1/\alpha$ in (a) and (b) respectively, with 1%, 5%, 10%, 20% noise. Each experiment is repeated 50 times and the error is averaged. The result shows that SC in this case is not sensitive to α , and there are a wide range choices of α that give rise to a small error.

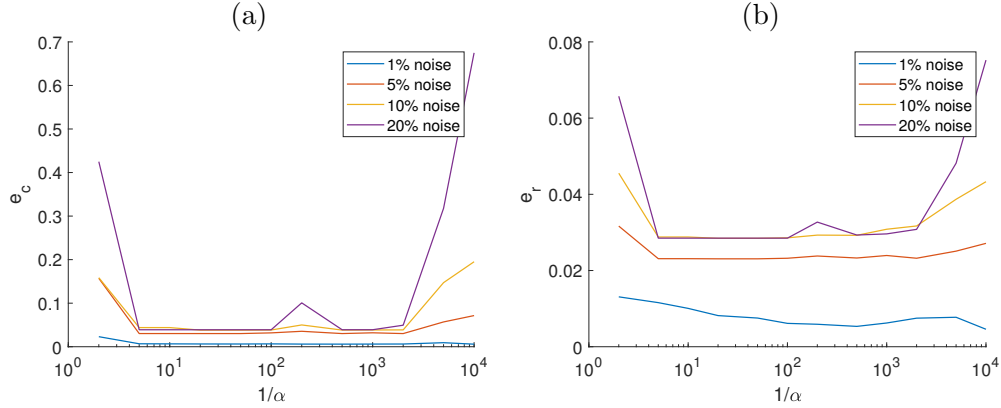


Figure 6: Robustness of SC to the choice of α for the recovery of the transport equation (12). (a) and (b) display e_c and e_r versus $1/\alpha$ respectively, with 1% (Blue), 5% (Red), 10% (Orange), 20% (Purple) noise. Each experiment is repeated 50 times and the errors are averaged. We observe that SC is not sensitive to α , and there are a wide range of values for α that give rise to a small error.

4.2 Burgers' Equation

In the second example, we test on the Burgers' equation, which is a first order nonlinear PDE:

$$u_t = -uu_x. \quad (13)$$

We use the initial condition $u_0 = \sin(4\pi x) \cos(\pi x)$ and zero Dirichlet boundary condition. Our data is generated by solving (13) with $\delta x = \Delta x = 1/256$, $\delta t = \Delta t = 10^{-3}$ and $T = 0.05$.

Method	Identified PDE, 0% noise without SDD	e_c	e_r
ST(20)	$u_t = -1.0023uu_x - 2.38 \times 10^{-5}u_xu_{xx}$	2.35×10^{-3}	5.07×10^{-3}
SC(1/500)	$u_t = -0.9960uu_x$	4.01×10^{-3}	2.58×10^{-3}
0% noise with SDD		e_c	e_r
ST(20)	$u_t = -1.0079uu_x - 0.0001u_xu_{xx}$	7.97×10^{-3}	1.43×10^{-2}
SC(1/500)	$u_t = -0.9888uu_x$	1.12×10^{-2}	7.20×10^{-3}
10% noise		e_c	e_r
ST(20) and SC(1/500)	$u_t = -1.0246uu_x$	2.46×10^{-2}	1.52×10^{-2}
40% noise		e_c	e_r
ST(20) and SC(1/500)	$u_t = -0.7366uu_x$	2.63×10^{-1}	1.64×10^{-1}

Table 3: Identification of the Burgers' equation (13) with different noise levels. The identification results by ST and SC are good with small e_c and e_r for a noise level up to 40%.

Table 3 shows the results of ST(20) and SC(1/500) with various noise levels. With clean data, ST identifies an additional term, but its coefficient is very small and the corresponding e_c and e_r are small. SC works very well on clean data. With 10% and 40% noise, both methods identify the same PDE with small e_c and e_r .

Figure 7 shows how e_c and e_r change when the noise level varies from 0.1% to 90%. Each experiment is repeated 50 times and the errors are averaged. We test IDENT, ST(20) and SC(1/500), and the results in Figure 7 show that ST and SC perform better than IDENT.

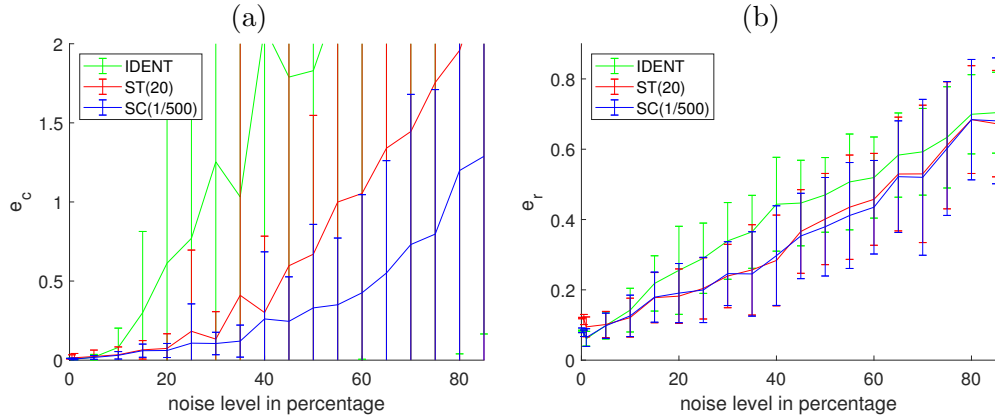


Figure 7: The average error e_c and e_r over 50 experiments of the Burgers' equation (13) with respect to various noise levels. (a) The curve represents the average e_c for IDENT [16] (Green), ST (Red) and SC (Blue), and the standard deviations are represented by vertical bars. (b) The average and variation of e_r for IDENT (Green), ST (Red) and SC (Blue). The e_c and e_r of ST and SC are much smaller than those of IDENT.

4.3 Burgers' Equation with Diffusion

Our third example is the Burgers' equation with diffusion, which is a second order nonlinear PDE:

$$u_t = -uu_x + 0.1u_{xx} . \quad (14)$$

We use the initial condition $u_0 = \sin(3\pi x) \cos(\pi x)$ and zero Dirichlet boundary condition. We first solve (14) with $\delta x = 1/256$, $\delta t = 10^{-5}$ and $T = 0.05$. The given data is downsampled from the numerical solution such that $\Delta x = 1/64$ and $\Delta t = 10^{-4}$.

Method	Identified PDE, 0% noise without SDD	e_c	e_r
ST(20) and SC(1/10)	$u_t = -1.0018uu_x + 0.1001u_{xx}$	1.67×10^{-3}	8.14×10^{-4}
	0% noise with SDD	e_c	e_r
ST(20) and SC(1/10)	$u_t = -0.9994uu_x + 0.1009u_{xx}$	1.36×10^{-3}	7.68×10^{-3}
	1% noise	e_c	e_r
ST(20) and SC(1/10)	$u_t = -0.9901uu_x + 0.1013u_{xx}$	1.02×10^{-2}	1.19×10^{-2}
	5% noise	e_c	e_r
ST(20) and SC(1/10)	$u_t = -1.0170uu_x + 0.0976u_{xx}$	1.77×10^{-2}	2.21×10^{-2}

Table 4: Identification of the Burgers' equation with diffusion (14) with different noise levels. The identification results by ST and SC are good with small e_c and e_r for a noise level up to 5%.

Table 4 shows the results of ST(20) and SC(1/10) with various noise levels. With clean data, 1% and 5% noise, both methods identify the PDE with small e_c and e_r .

Figure 8 shows how e_c and e_r change when the noise level varies from 0.1% to 10%. Each experiment is repeated 50 times and the error is averaged. We test IDENT, ST(20) and SC(1/10). Among the three methods, ST is the best. SC does not perform as well as ST and IDENT when noise level is large. For high order PDEs, the high order derivatives are heavily contaminated by noise, even with SDD, which affects the accuracy of cross validation. While ST and IDENT uses time evolution, it is easier to pick correct features. In general, ST performs better than SC for high order PDEs when the given data contain heavy noise.

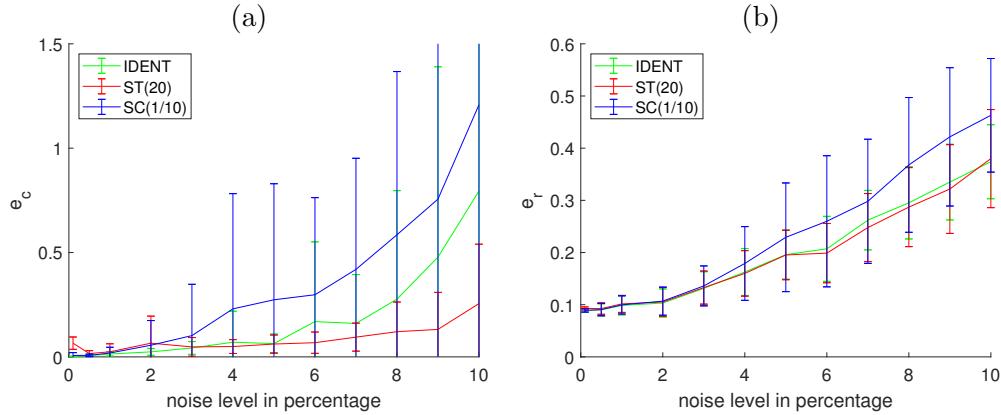


Figure 8: The average error e_c and e_r over 50 experiments of the Burgers' equation with diffusion (14) with respect to various noise levels. (a) The curve represents the average e_c for IDENT [16] (Green), ST (Red) and SC (Blue), and the standard deviations are represented by vertical bars. (b) The average and variation of e_r for IDENT (Green), ST (Red) and SC (Blue). Among the three methods, ST gives the best result.

In Figure 9, we explore the effect of α in SC on the Burgers' equation with diffusion. Figure 9 (a) and (b) show e_c and e_r versus $1/\alpha$ respectively, with 0.5%, 1%, 3%, 5% noise. When the noise level is low, such as 0.5% and 1%, we have a wide range of good choices of α which gives rise to a smaller error. As the noise level increases, the range of the optimal α becomes narrow.

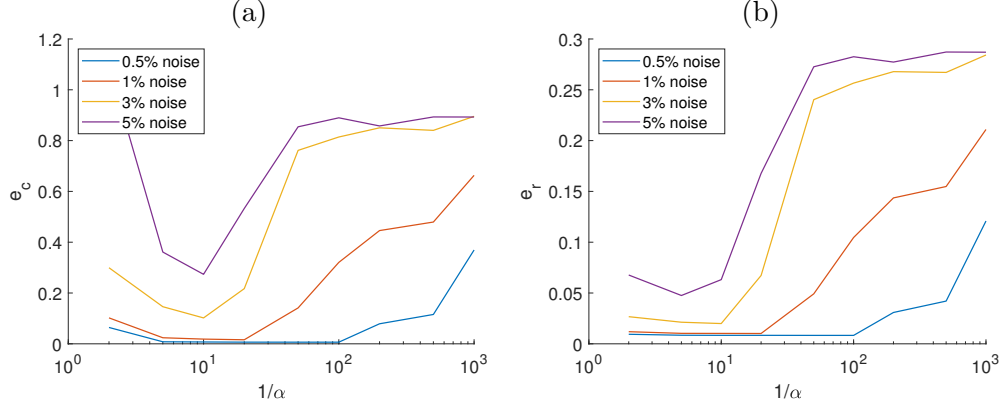


Figure 9: Robustness of SC to the choice of α for the recovery of the Burgers' equation with diffusion (14). (a) and (b) display e_c and e_r versus $1/\alpha$ respectively, with 0.5% (Blue), 1% (Red), 3% (Orange), 5% (Purple) noise. Each experiment is repeated 50 times and the errors are averaged. When the noise level is low, such as 0.5% and 1%, there are a wide range of values for α which give a small error. As the noise level increases, the range of the optimal α becomes narrow.

4.4 Two Dimensional PDEs

We apply our methods to identify two-dimensional PDEs. The PDEs are solved with $\delta x = \delta y = 0.02$ and $\delta t = 8 \times 10^{-4}$. Data are downsampled from the numerical solution with $\Delta x = 0.04$ and $\Delta t = 8 \times 10^{-3}$. We fix $w = 10$ for ST and $\alpha = 3/200$ for SC.

The identification of two-dimensional PDEs is more challenging and more sensitive to noise. There are more features in two dimensions, and the directional variation of the data adds complexity to the problem. We will show that both ST and SC are still robust against noise.

We first consider the following PDE:

$$\begin{cases} u_t = 0.02u_{xx} - uu_y \text{ for } (x, y, t) \in [0, 1]^2 \times [0, 0.1], \\ u(x, y, 0) = \sin^2(\frac{3\pi x}{0.9}) \sin^2(\frac{2\pi y}{0.9}) \text{ when } (x, y) \in [0, 0.9]^2 \text{ and } 0 \text{ otherwise.} \end{cases}, \quad (15)$$

which has different dynamics along the x and y directions. Table 5 shows the identification results of ST(10) and SC(3/200) with noise level 0%, 5% and 10%. Both methods identify the same features with small e_c and e_r .

Method	Identified PDE, 0% noise	e_c	e_r
ST(10) and SC(3/200)	$u_t = 0.0189u_{xx} - 0.9525uu_y$	4.75×10^{-2}	2.48×10^{-2}
	5% noise	e_c	e_r
ST(10) and SC(3/200)	$u_t = 0.0178u_{xx} - 0.9362uu_y$	8.43×10^{-2}	7.45×10^{-2}
	10% noise	e_c	e_r
ST(10) and SC(3/200)	$u_t = 0.0134u_{xx} - 0.8674uu_y$	1.33×10^{-1}	1.79×10^{-1}

Table 5: Identification of the two dimensional PDE (15) with different noise levels. The identification results by ST and SC have small e_c and e_r for a noise level up to 10%.

4.5 Identifiability Based on the Given Data

For the PDE identification, especially in high dimensions, the given data U plays an important role. When the initial condition has sufficient variations in each dimension, the correct PDE can

be identified. Otherwise, there may be multiple PDEs which generate the same dynamics. For example, consider the following transport equation without noise:

$$\begin{cases} u_t = -0.5u_x + 0.5u_y, & (x, y) \in [0, 1] \times [0, 1], \quad t \in [0, 0.1] \\ u(x, y, 0) = f(x, y), & (x, y) \in [0, 1] \times [0, 1] \end{cases}, \quad (16)$$

where f denotes the initial condition.

We first choose $f(x, y) = \sin(2\pi x/0.9)^2 \sin(2\pi y/0.9)^2$ for $(x, y) \in [0, 0.9] \times [0, 0.9]$ and 0 otherwise. The identified PDE by SC(3/200) is

$$u_t = -0.4995u_x + 0.4786u_y,$$

where the recovered coefficients are very close to the true coefficients. Next we choose $f(x, y) = \sin(2\pi x/0.9)^2$ for $(x, y) \in [0, 0.9] \times \mathbb{R}$ and 0 otherwise, then SC(3/200) gives

$$u_t = -0.4992u_x. \quad (17)$$

With this initial condition, the PDE in (16) has the exact solution:

$$u(x, y, t) = \begin{cases} \sin\left(\frac{2\pi(x-0.5t)}{0.9}\right)^2, & x \in [0.5t, 0.9 + 0.5t], \quad (x, y) \in \mathbb{R} \times [0, 1], \quad t \in [0, 0.1] \\ 0, & \text{Otherwise} \end{cases},$$

which also satisfies $u_t = -0.5u_x$. The identified PDE in (17) approximates this simpler equation. Since the given data only vary along the x direction, the columns in the feature matrix related to y , e.g., u_y , $u_x u_y$, and u_{yy} , are mostly 0. This explains why our method identifies the PDE in (17), instead of (16).

4.6 Choice of Smoother in SDD

In this paper, we use Moving Least Square (MLS) as the denoising in SDD. To numerically justify this choice among Moving Average (MA) [38], cubic spline interpolation [9], and diffusion smoothing [45], we present the SDD results with these smoothers in Figure 10. We first solve the PDE

$$u_t = -0.4uu_x - 0.2uu_y, \quad (x, y) \in [0, 1] \times [0, 1], \quad t \in [0, 0.15], \quad (18)$$

with $\Delta t = 0.005$ and $\Delta x = \Delta y = 0.01$, where the initial condition is $u_0(x, y) = \sin(3\pi x) \sin(5\pi y)$. Then 5% Gaussian noise is added on the numerical solution. Given the noisy data, we perform SDD denoising with different smoothers to obtain various partial derivatives. In MLS, we take the bandwidth $h = 0.04$. For MA, the window size for averaging is fixed to be 3. For Cubic Spline, we use the MATLAB function *csaps* with $p = 0.5$. For the Diffusion denoising, we evolve the noisy surface following the heat equation $u_t = u_{xx} + u_{yy}$ with a time step size $(\Delta x)^2/4$ for 5 iterations. Figure 10 shows the SDD results of u , u_x , u_{yy} , uu_x at $t = 0.15$ when different smoothers are used in SDD. All of them recover U (the first row), while MLS preserves the underlying dynamics the best, i.e. the first and second order derivatives.

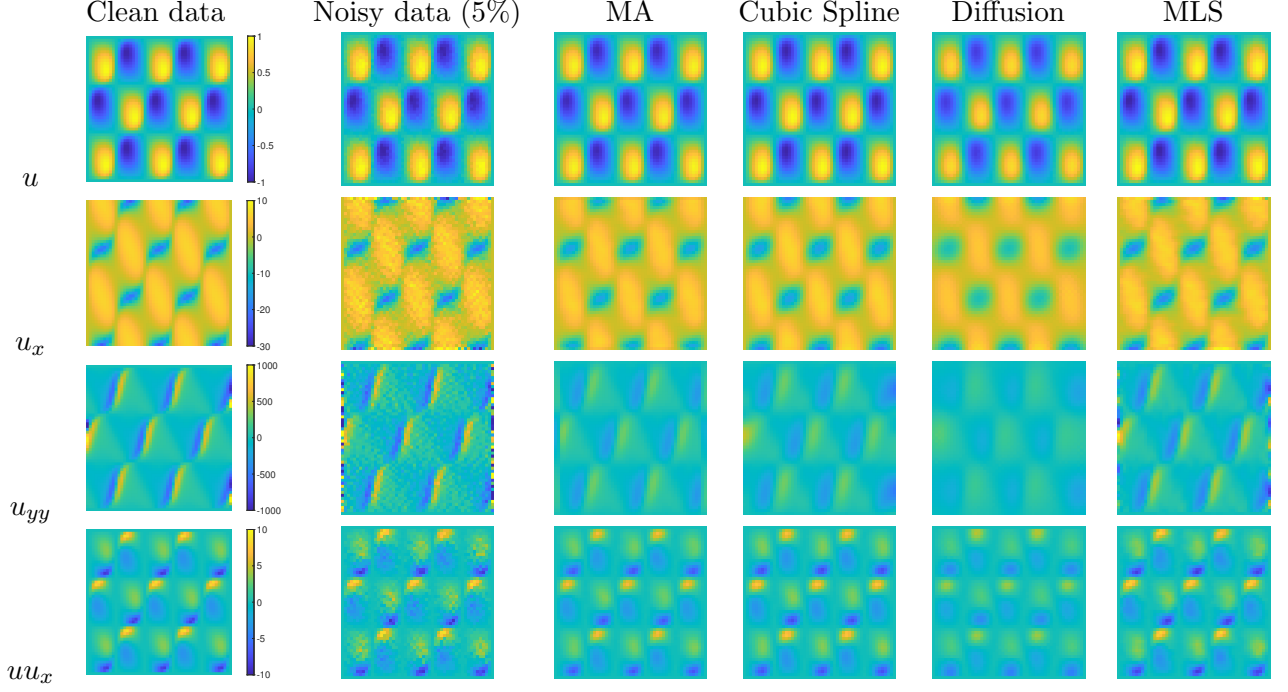


Figure 10: SDD results with different smoothers. The first column is the numerical solution of (18) at $t = 0.15$ with the initial condition $u_0(x, y) = \sin(3\pi x) \sin(5\pi y)$ and its various partial derivatives. The second column shows the noisy data and its numerical derivatives when 5% Gaussian noise is added to the clean data. The right four columns are the SDD results at $t = 0.15$ using MA, cubic spline, diffusion and MLS in order. While all methods recover U (the first row), the dynamics of the derivatives, especially in the third and forth rows, are best preserved by MLS.

5 Conclusion

This paper developed two robust methods for PDE identification when noisy data are given. First, we proposed a Successively Denoised Differentiation (SDD) procedure to stabilize numerical differentiation, which significantly improves the accuracy in the computation of the feature matrix from noisy data. We then proposed two new robust PDE identification algorithms called ST and SC. These algorithms utilize the Subspace Pursuit (SP) greedy algorithm to efficiently select a candidate set, and then refine the results by time evolution or cross validation. We presented various numerical experiments to demonstrate the effectiveness of both methods. SC is more computationally efficient, while ST performs better for PDEs with high order derivatives. We also provided an error analysis of ST and SC in the context of PDE identification, which unifies many related methods in the literature.

Appendix

A Relation between the Errors $e(u)$ and $e(u_t)$

In this section, we explain the statement in Section 3.3: If the numerical scheme for the computation of $D_t \hat{U}$ is consistent, then $\|e(u)\|_\infty \rightarrow 0$ and $\|e(u_t)\|_\infty \rightarrow 0$ are equivalent as $\Delta t, \Delta x \rightarrow 0$.

For $n = 0, 1, \dots, N$, we denote $e(u)^n$ and $e(u_t)^n$ as the values of $e(u)$ and $e(u_t)$ occurred at time

$n\Delta t$, respectively. For $j = 1, 2, \dots, N$, we have

$$\frac{e(u)^j - e(u)^{j-1}}{\Delta t} = \frac{\widehat{U}^j - \widehat{U}^{j-1}}{\Delta t} - u_t^{j-1} + \mathbf{r}' = e(u_t)^{j-1} + \left(\frac{\widehat{U}^j - \widehat{U}^{j-1}}{\Delta t} - [D_t \widehat{U}]^{j-1} \right) + \mathbf{r}' ,$$

where $\|\mathbf{r}'\|_\infty = O(\Delta t)$. By induction, we obtain the following connection between $e(u)$ and $e(u_t)$:

$$e(u)^n = e(u)^0 + \sum_{j=0}^{n-1} e(u_t)^j \Delta t + \sum_{j=0}^{n-1} \left(\frac{\widehat{U}^{j+1} - \widehat{U}^j}{\Delta t} - [D_t \widehat{U}]^j \right) \Delta t + n\mathbf{r} , \quad (19)$$

where the remainder $\|\mathbf{r}\|_\infty = O(\Delta t^2)$. Equation (19) suggests that if the approximation $D_t \widehat{U}$ is consistent and $\|e(u)^0\|_\infty$ converges to 0 as $\Delta x \rightarrow 0$, $\|e(u)\|_\infty \rightarrow 0$ is equivalent to $\|e(u_t)\|_\infty \rightarrow 0$. Therefore, the PDE identification methods with the goal of having $\|e(u)\|_\infty$ or $\|e(u_t)\|_\infty$ approach to 0 are equivalent.

It is often practical to consider a grid-dependent L_2 -norm of the errors, i.e., $\|\cdot\|_{2,\Delta} = \|\cdot\|_2 \sqrt{\Delta x \Delta t}$ where $\|\cdot\|_2$ denotes the ordinary L_2 vector norm. We provide an upper bound for $\|e(u)\|_{2,\Delta}$.

Theorem A.1. *Suppose $D_t \widehat{U}$ is computed using the forward difference. Then*

$$\|e(u)\|_{2,\Delta}^2 \leq X^d T^3 \|e(u_t)\|_\infty^2 + O(\|e(u_t)\|_\infty + \Delta t) + O(\Delta t) . \quad (20)$$

Proof. Recall that $U \in \mathbb{R}^{M^d N}$ is the vectorization of the data. By the definition of the grid-dependent norm, $\|U\|_{2,\Delta}^2 = \Delta x^d \Delta t \|U\|_2^2 = \frac{X^d T}{M^d N} \|U\|_2^2$. Using (19), we have

$$\begin{aligned} \|e(u)\|_2^2 &= \|e(u)^0\|_2^2 + \sum_{n=1}^N \|e(u)^n\|_2^2 \\ &\leq \|e(u)^0\|_2^2 + \sum_{n=1}^N \left(\sum_{j=0}^{n-1} \|e(u_t)^j\|_2 \right)^2 \Delta t^2 + M^d \sum_{n=1}^N n^2 O(\Delta t^4) + \\ &\quad \sum_{n=1}^N \|e(u)^0\|_2 \sum_{j=0}^{n-1} \|e(u_t)^j\|_2 \Delta t + M^{d/2} \sum_{n=1}^N \|e(u)^0\|_2 n O(\Delta t^2) + M^{d/2} \sum_{n=1}^N \sum_{j=0}^{n-1} \|e(u_t)^j\|_2 n O(\Delta t^3) \\ &\leq \|e(u)^0\|_2^2 + \sum_{n=1}^N \left(\sum_{j=0}^{n-1} \|e(u_t)^j\|_2 \right)^2 \Delta t^2 + M^d O(T^3 \Delta t) \\ &\quad + \|e(u)^0\|_2 \sum_{n=1}^N \sum_{j=0}^{n-1} \|e(u_t)^j\|_2 \Delta t + M^{d/2} \|e(u)^0\|_2 O(T^2) + M^{d/2} \sum_{n=1}^N \sum_{j=0}^{n-1} \|e(u_t)^j\|_2 n O(\Delta t^3) . \end{aligned}$$

Since $\|e(u_t)^j\|_2 \leq M^{d/2} \|e(u_t)\|_\infty$, we can simplify the expression above as:

$$\begin{aligned} \|e(u)\|_2^2 &\leq \|e(u)^0\|_2^2 + M^d T^2 N \|e(u_t)\|_\infty^2 + M^d O(T^3 \Delta t) \\ &\quad + T M^{d/2} N \|e(u)^0\|_2 \|e(u_t)\|_\infty + M^{d/2} \|e(u)^0\|_2 O(T^2) + M^d \|e(u_t)\|_\infty O(T^3) . \end{aligned}$$

Thus

$$\begin{aligned} \|e(u)\|_{2,\Delta}^2 &= \Delta x^d \Delta t \|e(u)\|_2^2 \leq \Delta t \|e(u)^0\|_2^2 + X^d T^3 \|e(u_t)\|_\infty^2 + O(X^d T^3 \Delta t^2) \\ &\quad (\|e(u_t)\|_\infty + \Delta t) \|e(u)^0\|_2 O(T^2 X^{d/2}) + X^d \|e(u_t)\|_\infty O(T^3 \Delta t) . \end{aligned}$$

□

The upper bound expressed in (20) depends on several properties of the computational domain Ω and the sampling grid: the resolution Δt and the domain size X, T . To derive useful information from Theorem A.1, we assume that $\|e(u_t)\|_\infty = O(\Delta t)$. This condition holds, for example, when we use first order forward difference and the underlying data is noiseless.

Corollary A.2. *When the time-space domain is fixed, i.e., $T > 0$ and $X > 0$, if $\|e(u_t)\|_\infty = O(\Delta t)$, we have*

$$\|e(u)\|_{2,\Delta} \rightarrow 0, \quad \Delta t, \Delta x \rightarrow 0, \quad (21)$$

This result suggests that, with the assumptions satisfied, increasing both time and space resolutions is a sufficient condition for controlling $\|e(u)\|_{2,\Delta} \rightarrow 0$. The convergence of $\|e(u)\|_{2,\Delta}$ as $\Delta t, \Delta x \rightarrow 0$ guarantees the success of the methods which minimize the data fidelity term, e.g., ST and IDENT in [16].

B Proof of Proposition 3.1

Proof.

$$\begin{aligned}
& [D_t U]^{\mathcal{T}_2} - [F]_{\mathcal{A}}^{\mathcal{T}_2} ([F]_{\mathcal{A}}^{\mathcal{T}_1})^\dagger [D_t U]^{\mathcal{T}_1} \\
&= [D_t U]^{\mathcal{T}_2} - [u_t]^{\mathcal{T}_2} + [u_t]^{\mathcal{T}_2} - [F]_{\mathcal{A}}^{\mathcal{T}_2} ([F]_{\mathcal{A}}^{\mathcal{T}_1})^\dagger [D_t U]^{\mathcal{T}_1} \\
&= \underbrace{[D_t U]^{\mathcal{T}_2} - [u_t]^{\mathcal{T}_2}}_{E_1} + [u_t]^{\mathcal{T}_2} - [F]_{\mathcal{A}}^{\mathcal{T}_2} ([F]_{\mathcal{A}}^{\mathcal{T}_1})^\dagger [u_t]^{\mathcal{T}_1} - \underbrace{[F]_{\mathcal{A}}^{\mathcal{T}_2} ([F]_{\mathcal{A}}^{\mathcal{T}_1})^\dagger ([D_t U]^{\mathcal{T}_1} - [u_t]^{\mathcal{T}_1})}_{E_2} \\
&= [u_t]^{\mathcal{T}_2} - ([F_0]_{\mathcal{A}}^{\mathcal{T}_2} + [F]_{\mathcal{A}}^{\mathcal{T}_2} - [F_0]_{\mathcal{A}}^{\mathcal{T}_2}) ([F]_{\mathcal{A}}^{\mathcal{T}_1})^\dagger [u_t]^{\mathcal{T}_1} + E_1 + E_2 \\
&= [u_t]^{\mathcal{T}_2} - [F_0]_{\mathcal{A}}^{\mathcal{T}_2} ([F]_{\mathcal{A}}^{\mathcal{T}_1})^\dagger [u_t]^{\mathcal{T}_1} - \underbrace{([F]_{\mathcal{A}}^{\mathcal{T}_2} - [F_0]_{\mathcal{A}}^{\mathcal{T}_2}) ([F]_{\mathcal{A}}^{\mathcal{T}_1})^\dagger [u_t]^{\mathcal{T}_1}}_{E_3} + E_1 + E_2 \\
&= \underbrace{[u_t]^{\mathcal{T}_2} - [F_0]_{\mathcal{A}_0}^{\mathcal{T}_2} ([F_0]_{\mathcal{A}_0}^{\mathcal{T}_1})^\dagger [u_t]^{\mathcal{T}_1}}_{=0} + ([F_0]_{\mathcal{A}_0}^{\mathcal{T}_2} ([F_0]_{\mathcal{A}_0}^{\mathcal{T}_1})^\dagger - [F_0]_{\mathcal{A}}^{\mathcal{T}_2} ([F]_{\mathcal{A}}^{\mathcal{T}_1})^\dagger) [u_t]^{\mathcal{T}_1} + E_1 + E_2 + E_3 \\
&= ([F_0]_{\mathcal{A}_0}^{\mathcal{T}_2} ([F_0]_{\mathcal{A}_0}^{\mathcal{T}_1})^\dagger - [F_0]_{\mathcal{A}}^{\mathcal{T}_2} ([F]_{\mathcal{A}}^{\mathcal{T}_1})^\dagger) [u_t]^{\mathcal{T}_1} + E_1 + E_2 + E_3 \\
&= ([F_0]_{\mathcal{A}_0}^{\mathcal{T}_2} ([F_0]_{\mathcal{A}_0}^{\mathcal{T}_1})^\dagger - [F_0]_{\mathcal{A}}^{\mathcal{T}_2} ([F_0]_{\mathcal{A}}^{\mathcal{T}_1})^\dagger) [u_t]^{\mathcal{T}_1} \\
&\quad - \underbrace{[F_0]_{\mathcal{A}}^{\mathcal{T}_2} (([F]_{\mathcal{A}}^{\mathcal{T}_1})^\dagger - ([F_0]_{\mathcal{A}}^{\mathcal{T}_1})^\dagger) [u_t]^{\mathcal{T}_1}}_{E_4} + E_1 + E_2 + E_3 \\
&= ([F_0]_{\mathcal{A}_0}^{\mathcal{T}_2} ([F_0]_{\mathcal{A}_0}^{\mathcal{T}_1})^\dagger - [F_0]_{\mathcal{A}}^{\mathcal{T}_2} ([F_0]_{\mathcal{A}}^{\mathcal{T}_1})^\dagger) [u_t]^{\mathcal{T}_1} + E_1 + E_2 + E_3 + E_4.
\end{aligned}$$

Then we have:

$$\begin{aligned}
\text{CEE}(\mathcal{A}_k; \alpha, \mathcal{T}_1, \mathcal{T}_2) &\leq \|([F_0]_{\mathcal{A}_0}^{\mathcal{T}_2} ([F_0]_{\mathcal{A}_0}^{\mathcal{T}_1})^\dagger - [F_0]_{\mathcal{A}}^{\mathcal{T}_2} ([F_0]_{\mathcal{A}}^{\mathcal{T}_1})^\dagger) [u_t]^{\mathcal{T}_1}\|_2 + \|[D_t U]^{\mathcal{T}_2} - [u_t]^{\mathcal{T}_2}\|_2 \\
&\quad + \|([F]_{\mathcal{A}}^{\mathcal{T}_1})^\dagger\|_2 (\|[F]_{\mathcal{A}}^{\mathcal{T}_2}\|_2 \|[D_t U]^{\mathcal{T}_1} - [u_t]^{\mathcal{T}_1}\|_2 + \|[F]_{\mathcal{A}}^{\mathcal{T}_2} - [F_0]_{\mathcal{A}}^{\mathcal{T}_2}\|_2 \|[u_t]^{\mathcal{T}_1}\|_2) \\
&\quad + \|[F_0]_{\mathcal{A}}^{\mathcal{T}_2}\|_2 \|([F]_{\mathcal{A}}^{\mathcal{T}_1})^\dagger\|_2 \|([F_0]_{\mathcal{A}}^{\mathcal{T}_1})^\dagger\|_2 \|[F]_{\mathcal{A}}^{\mathcal{T}_1} - [F_0]_{\mathcal{A}}^{\mathcal{T}_1}\|_2 \|[u_t]^{\mathcal{T}_1}\|_2.
\end{aligned}$$

In the last term on the right hand side of the inequality, we applied the norm bound in Theorem 4.1 of [43]. □

References

- [1] E. Baake, M. Baake, H. Bock, and K. Briggs. Fitting ordinary differential equations to chaotic data. *Physical Review A*, 45(8):5524, 1992.
- [2] M. Bär, R. Hegger, and H. Kantz. Fitting partial differential equations to space-time dynamics. *Physical Review E*, 59(1):337, 1999.
- [3] H. G. Bock. Numerical treatment of inverse problems in chemical reaction kinetics. In *Modelling of chemical reaction systems*, pages 102–125. Springer, 1981.
- [4] H. G. Bock. Recent advances in parameter identification techniques for ODE. In *Numerical treatment of inverse problems in differential and integral equations*, pages 95–121. Springer, 1983.
- [5] J. Bongard and H. Lipson. Automated reverse engineering of nonlinear dynamical systems. *Proceedings of the National Academy of Sciences*, 104(24):9943–9948, 2007.
- [6] M. Bongini, M. Fornasier, M. Hansen, and M. Maggioni. Inferring interaction rules from observations of evolutive systems i: The variational approach. *Mathematical Models and Methods in Applied Sciences*, 27(05):909–951, 2017.
- [7] S. L. Brunton, J. L. Proctor, and J. N. Kutz. Discovering governing equations from data by sparse identification of nonlinear dynamical systems. *Proceedings of the National Academy of Sciences*, 113(15):3932–3937, 2016.
- [8] E. J. Candès, J. Romberg, and T. Tao. Robust uncertainty principles: Exact signal reconstruction from highly incomplete frequency information. *IEEE Transactions on Information Theory*, 52(2):489–509, 2006.
- [9] P. Craven and G. Wahba. Smoothing noisy data with spline functions. *Numerische mathematik*, 31(4):377–403, 1978.
- [10] W. Dai and O. Milenkovic. Subspace pursuit for compressive sensing signal reconstruction. *IEEE transactions on Information Theory*, 55(5):2230–2249, 2009.
- [11] D. L. Donoho. Compressed sensing. *IEEE Transactions on Information Theory*, 52(4):1289–1306, 2006.
- [12] D. L. Donoho and X. Huo. Uncertainty principles and ideal atomic decomposition. *IEEE transactions on information theory*, 47(7):2845–2862, 2001.
- [13] A. Harten, B. Engquist, S. Osher, and S. R. Chakravarthy. Uniformly high order accurate essentially non-oscillatory schemes, iii. In *Upwind and high-resolution schemes*, pages 218–290. Springer, 1987.
- [14] T. Hastie, R. Tibshirani, and J. Friedman. *The elements of statistical learning: data mining, inference, and prediction*. Springer Science & Business Media, 2009.
- [15] E. Kaiser, J. N. Kutz, and S. L. Brunton. Sparse identification of nonlinear dynamics for model predictive control in the low-data limit. *Proceedings of the Royal Society A*, 474(2219):20180335, 2018.

- [16] S. H. Kang, W. Liao, and Y. Liu. IDENT: Identifying differential equations with numerical time evolution. *arXiv preprint arXiv:1904.03538*, 2019.
- [17] Y. Khoo and L. Ying. SwitchNet: a neural network model for forward and inverse scattering problems. *arXiv preprint arXiv:1810.09675*, 2018.
- [18] P. Lancaster and K. Salkauskas. Surfaces generated by moving least squares methods. *Mathematics of computation*, 37(155):141–158, 1981.
- [19] H. Liang and H. Wu. Parameter estimation for differential equation models using a framework of measurement error in regression models. *Journal of the American Statistical Association*, 103(484):1570–1583, 2008.
- [20] J.-C. Loiseau and S. L. Brunton. Constrained sparse galerkin regression. *Journal of Fluid Mechanics*, 838:42–67, 2018.
- [21] Z. Long, Y. Lu, and B. Dong. Pde-net 2.0: Learning pdes from data with a numeric-symbolic hybrid deep network. *Journal of Computational Physics*, 399:108925, 2019.
- [22] Z. Long, Y. Lu, X. Ma, and B. Dong. PDE-net: Learning PDSs from data. *arXiv preprint arXiv:1710.09668*, 2017.
- [23] F. Lu, M. Zhong, S. Tang, and M. Maggioni. Nonparametric inference of interaction laws in systems of agents from trajectory data. *Proceedings of the National Academy of Sciences*, 116(29):14424–14433, 2019.
- [24] B. Lusch, J. N. Kutz, and S. L. Brunton. Deep learning for universal linear embeddings of nonlinear dynamics. *Nature communications*, 9(1):4950, 2018.
- [25] N. M. Mangan, J. N. Kutz, S. L. Brunton, and J. L. Proctor. Model selection for dynamical systems via sparse regression and information criteria. *Proceedings of the Royal Society A: Mathematical, Physical and Engineering Sciences*, 473(2204):20170009, 2017.
- [26] T. Müller and J. Timmer. Parameter identification techniques for partial differential equations. *International Journal of Bifurcation and Chaos*, 14(06):2053–2060, 2004.
- [27] T. G. Müller and J. Timmer. Fitting parameters in partial differential equations from partially observed noisy data. *Physica D: Nonlinear Phenomena*, 171(1-2):1–7, 2002.
- [28] U. Parlitz and C. Merkwirth. Prediction of spatiotemporal time series based on reconstructed local states. *Physical review letters*, 84(9):1890, 2000.
- [29] T. Qin, K. Wu, and D. Xiu. Data driven governing equations approximation using deep neural networks. *Journal of Computational Physics*, 2019.
- [30] M. Raissi and G. E. Karniadakis. Hidden physics models: Machine learning of nonlinear partial differential equations. *Journal of Computational Physics*, 357:125–141, 2018.
- [31] M. Raissi, P. Perdikaris, and G. E. Karniadakis. Physics informed deep learning (part I): Data-driven solutions of nonlinear partial differential equations. *arXiv preprint arXiv:1711.10561*, 2017.
- [32] S. H. Rudy, S. L. Brunton, J. L. Proctor, and J. N. Kutz. Data-driven discovery of partial differential equations. *Science Advances*, 3(4):e1602614, 2017.

- [33] H. Schaeffer. Learning partial differential equations via data discovery and sparse optimization. *Proceedings of the Royal Society A: Mathematical, Physical and Engineering Sciences*, 473(2197):20160446, 2017.
- [34] H. Schaeffer, R. Caflisch, C. D. Hauck, and S. Osher. Sparse dynamics for partial differential equations. *Proceedings of the National Academy of Sciences*, 110(17):6634–6639, 2013.
- [35] H. Schaeffer, G. Tran, and R. Ward. Extracting sparse high-dimensional dynamics from limited data. *SIAM Journal on Applied Mathematics*, 78(6):3279–3295, 2018.
- [36] M. Schmidt and H. Lipson. Distilling free-form natural laws from experimental data. *science*, 324(5923):81–85, 2009.
- [37] S. W. Smith. *The Scientist and Engineer’s Guide to Digital Signal Processing*. California Technical Pub. San Diego, 1997.
- [38] M. Tham. Dealing with measurement noise. moving average filter. *Chemical Engineering and Advanced Materials, University of Newcastle upon Tyne*, 1998.
- [39] R. Tibshirani. Regression shrinkage and selection via the lasso. *Journal of the Royal Statistical Society: Series B (Methodological)*, 58(1):267–288, 1996.
- [40] J. Timmer, T. Müller, and W. Melzer. Numerical methods to determine calcium release flux from calcium transients in muscle cells. *Biophysical journal*, 74(4):1694–1707, 1998.
- [41] G. Tran and R. Ward. Exact recovery of chaotic systems from highly corrupted data. *Multiscale Modeling & Simulation*, 15(3):1108–1129, 2017.
- [42] H. U. Voss, P. Kolodner, M. Abel, and J. Kurths. Amplitude equations from spatiotemporal binary-fluid convection data. *Physical review letters*, 83(17):3422, 1999.
- [43] P.-Å. Wedin. Perturbation theory for pseudo-inverses. *BIT Numerical Mathematics*, 13(2):217–232, 1973.
- [44] H. Wendland. Local polynomial reproduction and moving least squares approximation. *IMA Journal of Numerical Analysis*, 21(1):285–300, 2001.
- [45] A. P. Witkin. Scale-space filtering. In *Readings in Computer Vision*, pages 329–332. Elsevier, 1987.
- [46] X. Xun, J. Cao, B. Mallick, A. Maity, and R. J. Carroll. Parameter estimation of partial differential equation models. *Journal of the American Statistical Association*, 108(503):1009–1020, 2013.
- [47] M. M. Zhang, H. Lam, and L. Lin. Robust and parallel bayesian model selection. *Computational Statistics & Data Analysis*, 127:229–247, 2018.